RESEARCH ARTICLE

WILEY

Study of NIT domain-containing chemoreceptors from two global phytopathogens and identification of NIT domains in eukaryotes

Elizabet Monteagudo-Cascales[1] | Álvaro Ortega[2] | Félix Velando[1] | Bertrand Morel[3] | Miguel A. Matilla[1] | Tino Krell [1]

[1]Department of Biotechnology and Environmental Protection, Estación Experimental del Zaidín, Consejo Superior de Investigaciones Científicas, Granada, Spain

[2]Department of Biochemistry and Molecular Biology 'B' and Immunology, Faculty of Chemistry, University of Murcia, Regional Campus of International Excellence 'Campus Mare Nostrum, Murcia, Spain

[3]Department of Physical Chemistry, Faculty of Sciences, University of Granada, Granada, Spain

Correspondence
Tino Krell and Miguel A. Matilla, Department of Biotechnology and Environmental Protection, Estación Experimental del Zaidín, Consejo Superior de Investigaciones Científicas, Prof. Albareda 1, 18008 Granada, Spain.
Email: tino.krell@eez.csic.es and miguel.matilla@eez.csic.es

Present address
Bertrand Morel, Angany Innovation, Val de Reuil, France

Funding information
Junta de Andalucía, Grant/Award Number: P18-FR-1621; Ministerio de Ciencia e Innovación, Grant/Award Number: PID2019-103972GA-I00, PID2020-112612GB-I00 and PID2021-122202OB-I00

Abstract

Bacterial signal transduction systems are typically activated by the binding of signal molecules to receptor ligand binding domains (LBDs), such as the NIT LBD. We report here the identification of the NIT domain in more than 15,000 receptors that were present in 30 bacterial phyla, but also in 19 eukaryotic phyla, expanding its known phylogenetic distribution. The NIT domain formed part of seven receptor families that either control transcription, mediate chemotaxis or regulate second messenger levels. We have produced the NIT domains from chemoreceptors of the bacterial phytopathogens *Pectobacterium atrosepticum* (PacN) and *Pseudomonas savastanoi* (PscN) as individual purified proteins. High-throughput ligand screening using compound libraries revealed a specificity for nitrate and nitrite binding. Isothermal titration calorimetry experiments showed that PacN-LBD bound preferentially nitrate ($K_D = 1.9\,\mu M$), whereas the affinity of PscN-LBD for nitrite ($K_D = 2.1\,\mu M$) was 22 times higher than that for nitrate. Analytical ultracentrifugation experiments indicated that PscN-LBD is monomeric in the presence and absence of ligands. The R182A mutant of PscN did not bind nitrate or nitrite. This residue is not conserved in the NIT domain of the *Pseudomonas aeruginosa* chemoreceptor PA4520, which may be related to its failure to bind nitrate/nitrite. The magnitude of *P. atrosepticum* chemotaxis towards nitrate was significantly greater than that of nitrite and *pacN* deletion almost abolished responses to both compounds. This study highlights the important role of nitrate and nitrite as signal molecules in life and advances our knowledge on the NIT domain as universal nitrate/nitrite sensor module.

KEYWORDS
bacterial signal transduction, chemoreceptor, chemotaxis, receptors, signal sensing

1 | INTRODUCTION

The capacity of bacteria to adapt to changing environmental conditions relies on an array of receptors that sense different signals. The major families of such receptors are sensor histidine kinases; chemoreceptors; adenylate, diadenylate and diguanylate cyclases; cAMP, c-di-AMP and c-di-GMP phosphodiesterases; protein kinases and phosphatases (Galperin, 2018). The canonical way by which these receptors are stimulated is via the binding of signal molecules to ligand binding domains (LBDs). Chemoreceptor-based signalling cascades are among the most complex prokaryotic signal transduction pathways that mediate chemotaxis, permitting bacteria to efficiently migrate in signal gradients. Typically, chemotactic signalling is initiated by signal recognition at the chemoreceptor LBD. Ligand binding causes a molecular stimulus that alters the autokinase activity of CheA and, consequently, the transphosphorylation of the response regulator CheY. In its phosphorylated state, CheY interacts with the flagellar motor, altering its activity and ultimately resulting in chemotaxis.

Based on the observation that signal affinities for full-length receptors and their individual LBDs are similar (Clarke & Koshland, 1979; Foster et al., 1985; Milligan & Koshland, 1993), LBDs are considered self-sufficient entities that contain all the requisites for ligand recognition. Hundreds of different LBDs have evolved (Matilla, Velando, Martín-Mora, et al., 2022; Mistry et al., 2021) and new LBDs are regularly discovered (Elgamoudi et al., 2021; Martin-Rodriguez et al., 2022). Members of one given LBD are frequently found in different receptor families (Shu et al., 2003; Ulrich & Zhulin, 2005), indicating that LBDs have been exchanged and recombined with different receptor families during evolution.

In 2003, The NIT-type LBD was predicted to be a nitrate-responsive module in bacterial sensory receptors (Shu et al., 2003). However, experimental evidence for this prediction is scarce. The existence of a bacterial LBD dedicated to sensing nitrate may be justified by the important physiological relevance of this ligand that was shown to: (i) support bacterial growth as the sole N-source (Kutvonen et al., 2015); (ii) function as a terminal electron acceptors for fermentation (Kraft et al., 2011) and (iii) act as a signal molecule (Gushchin et al., 2017). We have shown previously that the NIT domain of *Pseudomonas aeruginosa* chemoreceptor PA4520 does not bind nitrate/nitrite nor is it involved in mediating nitrate chemotaxis (Martín-Mora et al., 2019). In contrast, another study showed that the NIT domain of chemoreceptor Dd15070 from *Dickeya dadantii* bound nitrate with an affinity that was only slightly superior to that of nitrite (Gálvez-Roldán et al., 2022). NIT domains are found in more than 1% of chemoreceptors (Sanchis-López et al., 2021), and the 3D structure of an apo-NIT domain from the transcription anti-terminator NasR has been reported (Boudes et al., 2012) (Figure 1).

Here we have studied NIT domains from chemoreceptors of the plant pathogens *Pseudomonas savastanoi* pv. *savastanoi* and *Pectobacterium atrosepticum* that are both among the most relevant phytopathogens (Mansfield et al., 2012). Whereas *P. savastanoi* pv.
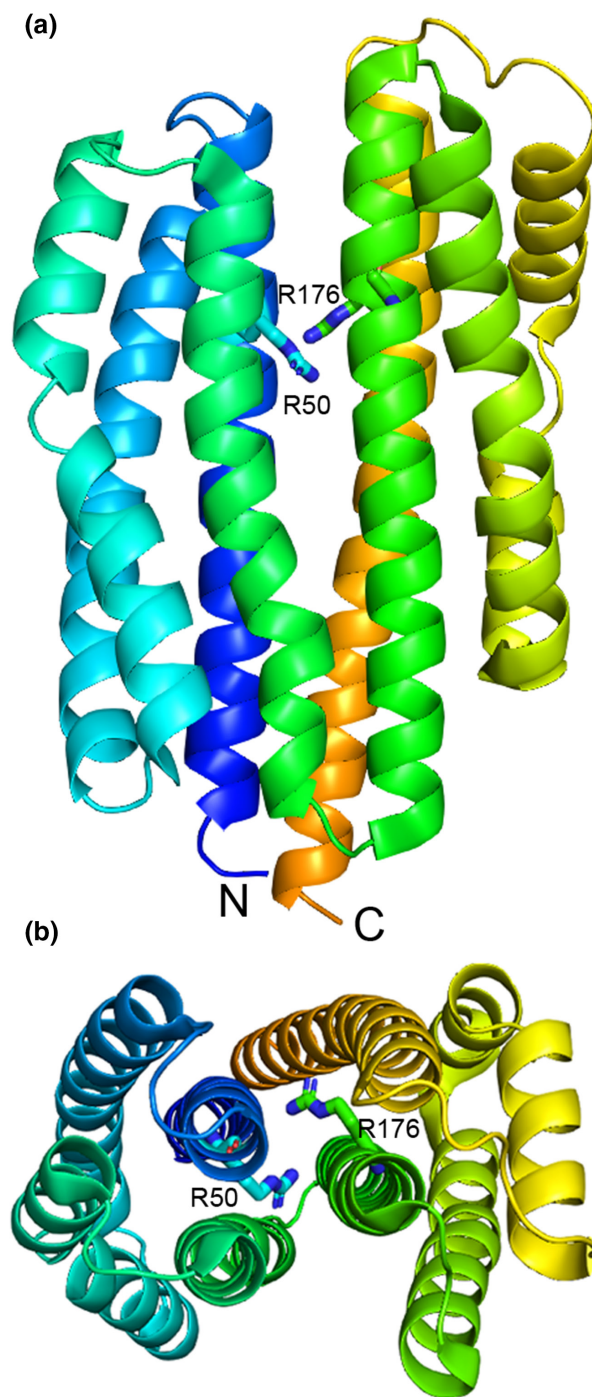
(a)

R176
R50

N   C

(b)

R176
R50

FIGURE 1 Three-dimensional structure of the NIT domain from the transcription anti-terminator NasR. (a) side view, (b) top view. The two arginine residues proposed to be involved in nitrate/nitrite recognition are shown in stick mode (Boudes et al., 2012). The structure is deposited in the protein data bank with ID 4AKK.

savastanoi is the causal agent of olive knot disease causing aerial tumours (Ramos et al., 2012), *P. atrosepticum* is responsible for the economically important blackleg and soft rot diseases (Toth, 2022). This research is embedded in efforts to identify the function of chemoreceptors in plant pathogens of global relevance. Plant pathogens contain on average 27 chemoreceptors (Sanchis-López

et al., 2021), a number that is significantly above the bacterial average of 15 (Sanchis-López et al., 2021). Bioinformatic analyses showed that many of these chemoreceptors are specifically found in plant-associated bacteria, suggesting that they recognise plant-derived compounds (Sanchis-López et al., 2021). However, there is very little information available on the function of phytopathogen chemoreceptors. In the context of plant infection, chemotaxis to compounds released from wounds and stomata is required for efficient plant entry and optimal virulence (Matilla & Krell, 2018). It was also shown that Interfering with chemotaxis on the leaf surface, by applying chemoattractants or masking existing compound gradients, reduces virulence (Cerna-Vargas et al., 2019; Tunchai et al., 2021). The prevention of bacterial stomatal entry is considered a promising alternative strategy to fight plant pathogens (Sakata & Ishiga, 2023). None of the 49 chemoreceptors of *P. savastanoi* pv. *savastanoi* NCPPB 3335 has so far been annotated with a function, but the role of specific chemoreceptors in plant virulence of this strain has been established (Matas et al., 2012). Alternatively, three of the 36 *P. atrosepticum* SCRI1043 chemoreceptors have been characterised. We have shown that PacA primarily mediates chemotaxis to the quaternary amines choline, betaine and L-carnitine (Matilla, Velando, Tajuelo, et al., 2022), which are important osmo- and thermo-protectants (Caldas et al., 1999; Chen & Beattie, 2008; Meadows & Wargo, 2015). PacB and PacC were identified as amino acid-responsive chemoreceptors with a wide or narrow ligand

profile, respectively (Velando et al., 2023). Both strains possess a single chemoreceptor with a NIT domain (Gumerov et al., 2020).

In the initial part of this study, we analysed the abundance of the NIT domains in different receptor families and determined their phylogenetic distribution. We then conducted a series of biophysical experiments with the individual NIT domain from chemoreceptors of *P. savastanoi* pv. *savastanoi* and *P. atrosepticum*. Finally, we conducted quantitative capillary chemotaxis assays to monitor cellular responses. The data obtained provided novel insights into this abundant but poorly characterised domain family.

2 | RESULTS

2.1 | NIT domains are found in eukaryotic and prokaryotic receptors

We retrieved the totality of NIT domain-containing proteins from the Pfam database (Mistry et al., 2021). Of the 15,400 NIT domain-containing sequences, about 500 were from eukaryotes, distributed over 19 different phyla (Figure 2, Data S1). NIT domains have been proposed to be bacterial sensor modules (Shu et al., 2003) and these data expand the phylogenetic spread of NIT domains. In almost all cases, the eukaryotic NIT domains formed part of guanylate cyclases (Pfam family: PF00211) that are enzymes involved in the synthesis
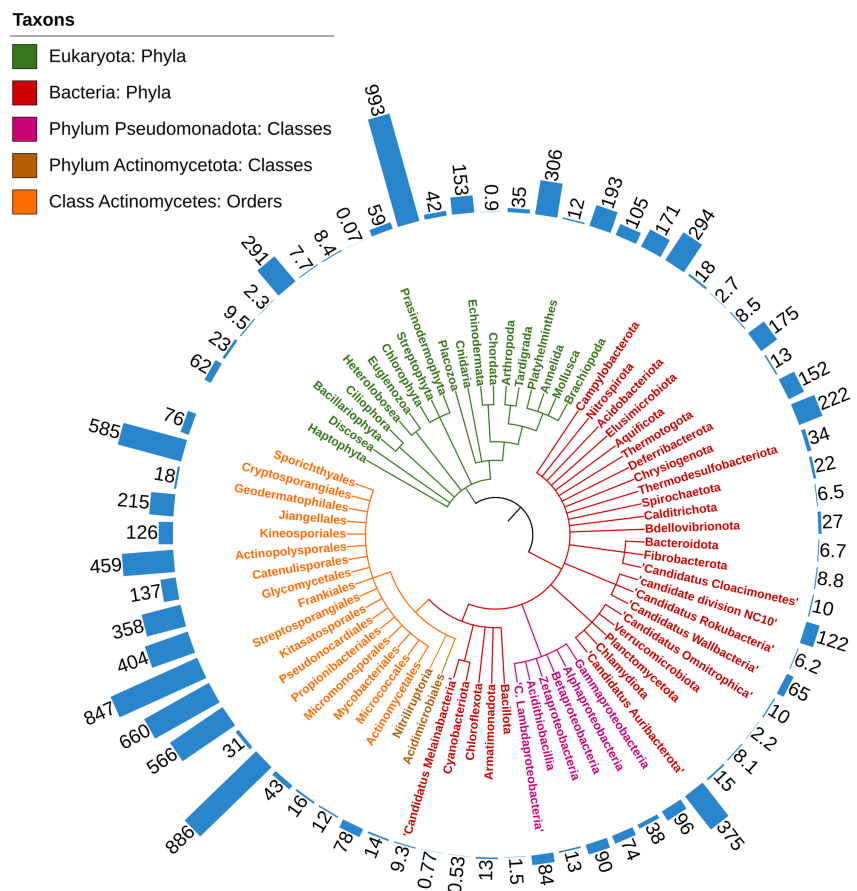

FIGURE 2 Phylogenetic distribution of NIT domain-containing proteins. The outer circle corresponds to the number of NIT domain-containing proteins over the total number of proteins multiplied by 1,000,000.

of the second messenger cGMP (Derbyshire & Marletta, 2012). Eukaryotic NIT-containing receptors are particularly abundant in Placozoa, millimetre-sized marine animals considered the simplest known free-living animals with only six morphologically recognised cell types (Schierwater et al., 2021; Smith et al., 2014). Placozoa are an essential taxon to comprehend the origin and evolution of animal life (Varoqueaux & Fasshauer, 2017). Furthermore, eukaryotic NIT domains were detected at important levels in Tardigrada (insects), Heterolobosea (Protista), Annelida (segmented worms), Echinodermata (the phylum to which sea urchins and starfish belong) or Brachiopoda (shells) (Figure 2). NIT domains were identified in 30 bacterial phyla but were absent from archaea (Figure 2). These domains were particularly abundant in Actinomycetota that harbour about 60% of the total number of NIT domains (almost 9300 sequences, Data S1). NIT domains are also found in all major classes of Pseudomonadota (Figure 2).

2.2 | More than half of all NIT domains form part of histidine sensor kinases

During evolution, LBDs have been exchanged among different receptor families (Shu et al., 2003; Ulrich & Zhulin, 2005). We have classified the NIT domains according to their respective receptor family (Figure 3). Twenty per cent of NIT domains are present in chemoreceptors, whereas the majority of NIT domains are found in two receptor families that control transcription, namely sensor histidine kinases (about 50%) and transcription anti-terminators (about 10%) (Figure 3). The remaining receptor families are primarily involved in the control of the homeostasis of the second messengers cAMP, cGMP and c-di-GMP (Figure 3). The primary physiological relevance of chemotaxis is to access nutrients (Colin et al., 2021), suggesting that this is likely to be the main function of NIT domain-containing chemoreceptors. However, these data also suggest that nitrate and nitrite are important signal molecules that control
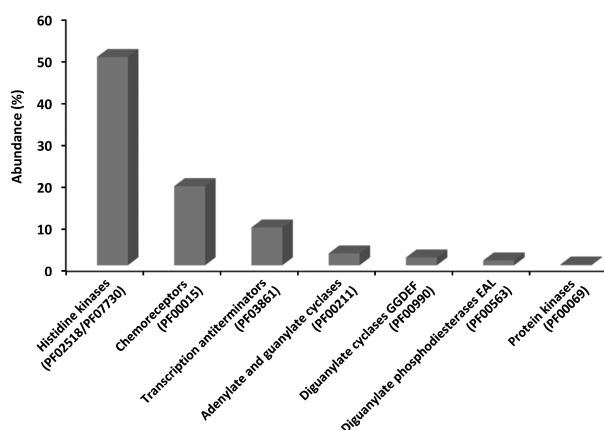
transcriptional activity and second messenger levels. A number of bacterial LBD families have been shown to be almost exclusively present in a given cellular compartment, such as the very abundant Cache or PAS families, that are either present in the extracytosolic space or cytosol, respectively (Upadhyay et al., 2016). In contrast, the NIT domain is present in both cellular compartments. Whereas transcription anti-terminators are cytosolic proteins, the majority of the remaining protein families possess extracytosolic NIT domains (Figure 3) (Shu et al., 2003).

2.3 | NIT domains differ in their ligand preferences for nitrate or nitrite

The NIT domain of the Dd15070 chemoreceptor from *Dickeya dadantii* had a preference for nitrate and bound nitrite with lower affinity (Gálvez-Roldán et al., 2022). To assess ligand specificity and affinity of NIT domains, we have produced the NIT domain of the chemoreceptor PSA3335_RS14925 from *P. savastanoi* pv. *savastanoi* NCPPB 3335 as a purified recombinant protein. To study ligand binding, we have conducted high-throughput thermal shift assays using the PM1, PM2A, PM3B, PM4A, PM5 and PM9 compound arrays from Biolog comprising 570 compounds corresponding to different carbon-, nitrogen-, phosphorous-, sulphur sources, nutrients and osmolytes. These assays determine ligand binding-induced increases in the protein thermal stability. Increases in the midpoint of protein folding transition (Tm) greater than 2°C are considered significant. Of all the compounds screened, there were only two ligands, nitrate and nitrite, that caused significant increases in the Tm, as shown in Figure 4a for the 95 compounds of compound array PM3B. Nitrite caused significantly larger increases than nitrate (Figure 4a). We renamed PSA3335_RS14925 chemoreceptor as PscN (*Pseudomonas savastanoi* chemoreceptor for nitrate/nitrite).

We subsequently studied the thermal unfolding of PscN-LBD in the absence and presence of nitrate and nitrite by differential scanning calorimetry. In analogy to the above data, nitrite induced larger increases in Tm (Figure 4b,c, Table S1). In addition, unfolding in the presence of nitrite was of higher cooperativity as compared to nitrate, as evidenced by a smaller peak width at half height of the unfolding transition (Table S1). Ligand binding to the NIT domain will induce structural alterations that trigger downstream signalling. To monitor ligand-induced structural changes, we have conducted far-UV circular dichroism spectroscopy studies (Figure 4d). The deconvolution of secondary structure elements indicated that the domain is largely helical (Table S2), consistent with the structures reported (Boudes et al., 2012). The addition of saturating concentrations of nitrate and nitrite induced only very minor changes, indicating that ligand binding does not induce large changes to the protein secondary structure (Figure 4d, Table S2). We subsequently conducted isothermal titration studies to derive the corresponding binding constants (Figure 5a, Table 1). Whereas the dissociation constant (K_D) of nitrite was $2.1\pm0.1\,\mu$M, nitrate bound with an about 22-fold lower affinity

FIGURE 3 Relative abundance of NIT domains in different families of signal transduction receptors. The total number of NIT domain-containing proteins as recovered from Pfam was considered 100%.
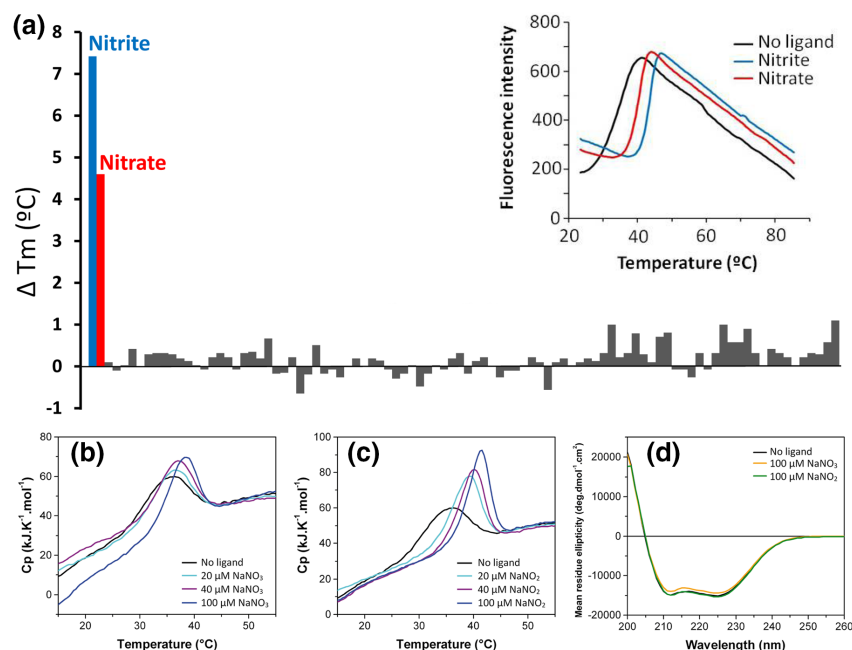
FIGURE 4 Ligand binding at PscN-LBD studied by thermal shift assays (a), differential scanning calorimetry (b, c) and circular dichroism spectroscopy (d). (a) Increases in the midpoint of thermal unfolding transition (Tm) in the presence of compounds of the PM3B array (Biolog, Hayward CA, USA) as compared to the ligand-free protein (Tm=34.7°C). The insert shows the raw data. (b, c) Differential scanning calorimetry data of the protein in the absence and presence of different concentrations of nitrate and nitrite. The derived thermodynamic parameters of protein unfolding are provided in Table S1. (d) Far-UV circular dichroism spectra of the protein in the absence and presence of NaNO$_3$ and NaNO$_2$. The relative abundance of derived secondary structure elements is provided in Table S2.

FIGURE 5 Microcalorimetric titration of the PscN-LBD and PacN-LBD with nitrate and nitrite. (a) Titration of 13–19 µM PscN-LBD with 3.2 µL aliquots of 400 µM NaNO$_2$ or 2 mM NaNO$_3$. (b) Titration of 20 µM PacN-LBD with 3.2 µL aliquots of 1 mM NaNO$_2$ or 1 mM NaNO$_3$. Upper panels: Raw titration data. Lower panels: Concentration-normalised and dilution heat-corrected integrated raw data. The line corresponds to the best fit using the 'one binding site model' of the MicroCal version of ORIGIN. The derived dissociation constants are indicated.
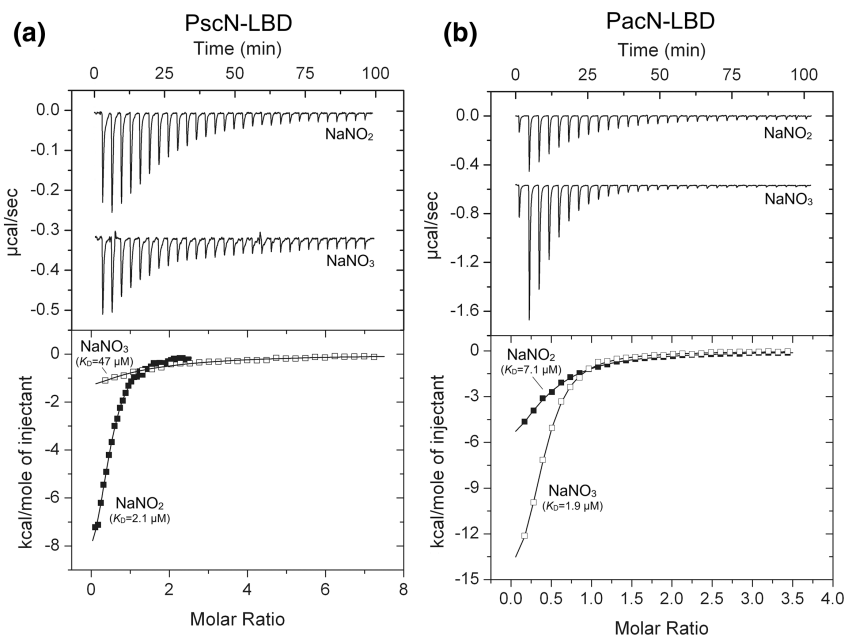
($K_D=47\pm7\,µM$). These data indicate that PscN-LBD is specific for nitrate and nitrite, but binds the latter with strong preference.

Considering that the ligand preferences differ between Dd15070-LBD (Gálvez-Roldán et al., 2022) and PscN-LBD, we studied the NIT domain of the chemoreceptor ECA_RS02210 from *P. atrosepticum* SCRI1043. To this end, we used a similar approach

and produced the individual domain as purified protein for its microcalorimetric analysis. In contrast to PscN-LBD, this domain bound preferentially nitrate ($K_D=1.9\pm0.1\,µM$) and nitrite with lower affinity ($K_D=7.1\pm0.3\,µM$) (Figure 5b). This chemoreceptor was named PacN (*Pectobacterium atrosepticum* chemoreceptor for nitrate/nitrite).

Protein	Strain	Ligand	ΔTm (°C)	K_D (μM)
PscN-LBD	*P. savastanoi* pv. *savastanoi* NCPPB 3335	NaNO$_3$	4.6	47 ± 7
PscN-LBD	*P. savastanoi* pv. *savastanoi* NCPPB 3335	NaNO$_2$	7.4	2.1 ± 0.1
PacN-LBD	*P. atrosepticum* SCRI1043	NaNO$_3$	n.d.	1.9 ± 0.1
PacN-LBD	*P. atrosepticum* SCRI1043	NaNO$_2$	n.d.	7.1 ± 0.3
PscN-LBD R182A	*P. savastanoi* pv. *savastanoi* NCPPB 3335	NaNO$_3$	0	No binding
PscN-LBD R182A	*P. savastanoi* pv. *savastanoi* NCPPB 3335	NaNO$_2$	0	No binding
PA4520-LBD	*P. aeruginosa* PAO1	NaNO$_3$	n.d.	No binding[a]
PA4520-LBD	*P. aeruginosa* PAO1	NaNO$_2$	n.d.	No binding[a]

TABLE 1 Binding studies of nitrate and nitrite to the individual NIT domains of chemoreceptors.

Note: Increases in Tm values were derived from thermal shift assays and Dissociation constants (K_D) are derived from microcalorimetric titrations.

Abbreviation: n.d., not determined.

[a]Reported previously in Martín-Mora et al. (2019).

2.4 | PscN-LBD is monomeric in the absence and presence of ligand

Analyses of different LBDs have shown that there are two different sensing mechanisms. Some LBDs, like members of the HBM or four-helix bundle families, are dimeric and recognise their signal at the dimer interface in a way that the bound signal contacts with both protein chains. For those domains, ligand binding typically causes dimer stabilisation (Fernández et al., 2017; Hida et al., 2017; Lacal et al., 2010; Martin-Mora et al., 2016; Monteagudo-Cascales et al., 2022; Pineda-Molina et al., 2012). Frequently, ligands bind with negative cooperativity to both binding sites of the dimer (Biemann & Koshland Jr., 1994; Ottemann & Koshland, 1997; Yu et al., 2015; Zhang et al., 2005) and it was proposed that negative cooperativity plays an important role in signalling since it permits highly ultrasensitive responses and the establishment of pronounced thresholds (Ha & Ferrell, 2016). Other LBDs, such as members of the dCache domain family, are monomeric and bound ligands that establish contacts with a single protein chain, in a process where ligand binding does not trigger domain dimerisation (Gavira et al., 2018; Rico-Jiménez et al., 2013). However, no information on the NIT sensing mode is available.

To assess this issue we have conducted analytical ultracentrifugation studies of PscN-LBD in the presence and absence of nitrate and nitrite. Experiments at different protein concentrations (5–20 μM) in the absence of the cognate ligands showed a single peak corresponding to a standard sedimentation coefficient of $s = 2.7$ S, independently of the protein concentration (Figure 6; note: this figure represents the sedimentation-coefficient values recorded in buffer, whereas standard sedimentation-coefficient values are normalised for migration in water at 20°C). Furthermore, the frictional ratio of 1.35 reflected that PscN-LBD is an elongated protein. The molecular weight of 30 kDa was derived from the combination of the sedimentation coefficient and the frictional ratio values. This is very close to the sequence-derived mass (31.8 kDa), showing that the
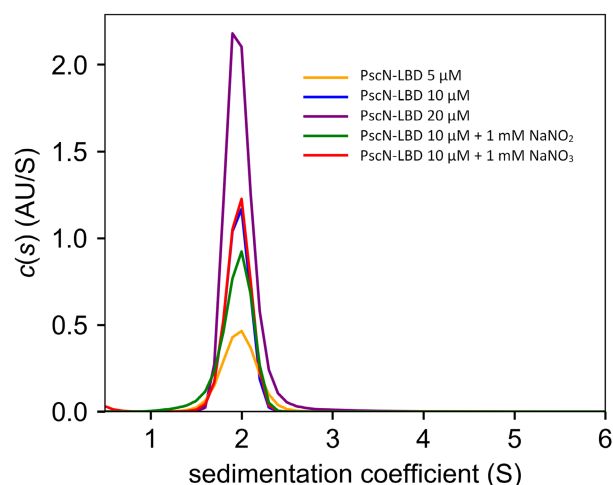

FIGURE 6 Sedimentation-velocity analytical ultracentrifugation studies of PscN-LBD. Sedimentation-coefficient profiles at different protein concentrations in the absence and presence of NaNO$_2$ or NaNO$_3$.

PscN-LBD is monomeric. The addition of saturating concentrations of nitrate and nitrite did not induce any alteration in the sedimentation coefficient (Figure 6), indicating that ligand binding does not induce the generation of oligomeric species.

2.5 | R182 of PscN-LBD is essential for ligand recognition

Following the demonstration that PscN and PacN bound nitrate and nitrite, we returned to the issue that the NIT domain of *P. aeruginosa* chemoreceptor PA4520 failed to bind any of these ligands and consequently did not mediate nitrate chemotaxis (Martín-Mora

FIGURE 7 Binding studies of nitrate and nitrite to PscN-LBD_R182A. (a, b) Thermal shift assays of PscN-LBD_R182A in the absence and presence of 1 mM $NaNO_2$ or $NaNO_3$. (a) Raw data. (b) First derivatives of the raw data. The minima correspond to the midpoints of the protein unfolding transition (Tm). (c) Microcalorimetric titrations of buffer and PscN-LBD_R182A with $NaNO_2$ and $NaNO_3$.
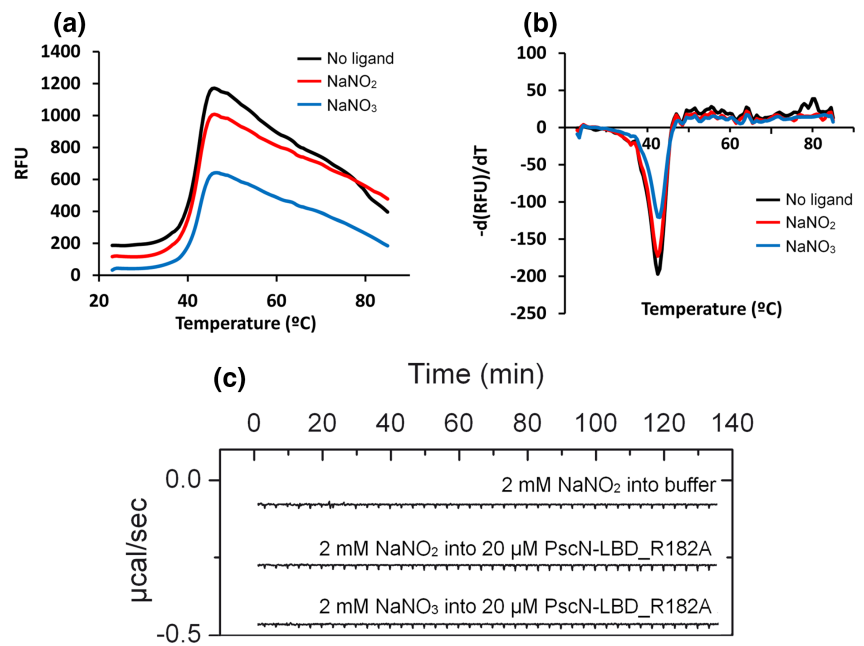
et al., 2019). The analysis of the NasR structure suggested that R50 and R176 are key residues for nitrate/nitrite recognition (Boudes et al., 2012) (Figure 1). A sequence alignment of the NIT domains from NasR, PscN, PacN and PA4520 showed that NasR R50 was fully conserved (Figure S1). In contrast, NasR R176 was conserved in PscN and PacN, but not in PA4520. To analyse the role of this residue in ligand recognition, we generated the alanine substitution mutant of the corresponding residue in PscN (PscN-LBD_R182A). Three-dimensional models of PscN-LBD and PA4520-LBD generated with Alphafold (Jumper et al., 2021) illustrate the position of these arginine residues (Figure S2). Thermal shift assays and isothermal titration calorimetry experiments showed that PscN-LBD_R182A is devoid of ligand binding (Figure 7). The non-conservation of this residue in PA4520 may thus be the cause for its failure to bind nitrate/nitrite. The NIT domain family may thus contain members that do not bind nitrate or nitrite, and such proteins could potentially be identified by the lacking conservation of this arginine residue. To identify the ligand recognised by PA4520-LBD, we have conducted thermal shift assays using compound arrays PM1, PM2A, PM3B, PM4A, PM5 and PM9. However, no significant Tm shifts were observed and further research is required to identify the signal(s) recognised by PA4520-LBD.

2.6 | PacN-mediated chemoattraction to nitrate is largely superior to that of nitrite

We have shown previously that *P. atrosepticum* SCRI1043 performs strong chemotaxis to nitrate under nitrogen-limiting conditions, whereas almost no chemotaxis was observed under nitrate-abundant conditions (Martín-Mora et al., 2019). To determine the role of PacN in this process, we have generated the corresponding deletion mutant. Initial quantitative capillary chemotaxis assays showed that the

response of the wild-type and mutant strains to casamino acids, mediated by other receptors (Velando et al., 2023), were comparable (Figure S3). In subsequent experiments, we assessed the response of the wild-type strain to nitrate and nitrite (Figure 8). Very strong chemotaxis was observed for nitrate, whereas maximal responses to nitrite were about 13-fold lower over the entire concentration range analysed, indicative of a clear preference for nitrate. Under all conditions, the response of the *pacN* mutant was significantly lower as compared to the wild-type strain, indicating that PacN is the primary nitrate/nitrite chemoreceptor in SCRI1043. The residual activity of the mutant strain, particularly pronounced at 5 mM nitrate (Figure 8), suggests the existence of an additional, low-sensitivity chemoreceptor.

3 | DISCUSSION

In the initial report, NIT domains were identified in prokaryotes (Shu et al., 2003). Here we show that NIT domains are present in 19 different eukaryotic phyla. A recent study reported the identification of 12 NIT domain-containing guanylate cyclases in the eukaryotic phylum Placozoa (Moroz et al., 2020). The homology model of eukaryotic NIT domains was highly similar to the NIT domain structure (Moroz et al., 2020), including the conservation of two arginine residues required for nitrate sensing mentioned above (Figure S1) (Moroz et al., 2020), suggesting that these domains also respond to nitrate/nitrite. Here, we show that Placozoa are by the far the eukaryotic phylum with the highest abundance of NIT domains. Placozoa are considered the simplest animals. They do not possess a nervous system, but different cell types were found to communicate (Varoqueaux et al., 2018). In this context, Placozoa have a rich receptor repertoire that senses a large number of different signals (Ringrose et al., 2013; Varoqueaux et al., 2018;
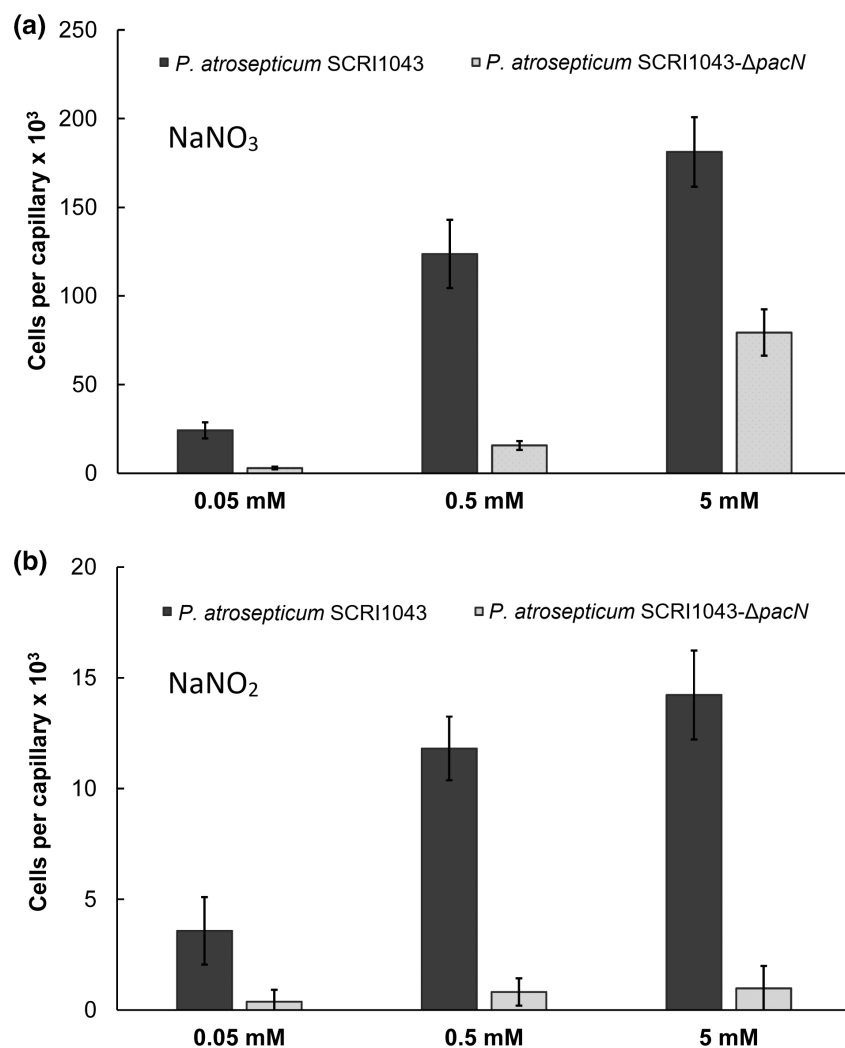
FIGURE 8 Chemotaxis of *P. atrosepticum* and the mutant deficient in the *pacN* gene towards different concentration of nitrate (a) and nitrite (b). Data have been corrected for the number of bacteria that swam into capillaries containing buffer (NaNO$_3$; 2346±751 for wt strain and 1869±622 for *pacN* mutant; NaNO$_2$: 2487±318 for wt strain and 1936±377 for *pacN* mutant). Data are means and standard deviations from three independent experiments conducted in triplicate.

Yañez-Guerra et al., 2022) and NIT domain-containing receptors in Placozoa were proposed to participate in NO-mediated signalling processes (Moroz et al., 2020, 2021). In addition, NIT domains are found in 18 other eukaryotic phyla (Figure 2). In prokaryotic organisms, NIT domains were particularly abundant in Actinomycetotas, which are Gram-positive bacteria widely present in the soil and aquatic ecosystems (van Bergeijk et al., 2020). The abundance of NIT domains in Actinomycetotas may be related to their capacity to perform anaerobic (Shoun et al., 1998) and aerobic denitrification (Zhang et al., 2021). In the initial report, NIT domains have been identified in four protein families, namely sensor histidine kinases, chemoreceptors, transcription anti-terminators and diguanylate cyclases and phosphodiesterases (Shu et al., 2003). In our study we have detected NIT domains in two additional families, adenylate/ guanylate cyclases and protein kinases (Figure 3), indicating that NIT domains-based sensing is involved in different processes such as chemotaxis, transcriptional regulation and the control of various second messenger levels.

The NIT domain is an atypical sensor domain. Whereas typically members of a given extracytosolic sensor domain family bind a variety of structurally different ligands (Matilla, Velando, Martín-Mora

et al., 2022), the NIT domain was predicted to be specific for nitrite (Shu et al., 2003). Our thermal shift assay-based ligand screening experiments of PscN-LBD confirm this prediction (Figure 4). Of the 570 compounds that we used for ligand screening, only nitrate and nitrite produced significant shifts. Among the ligands tested were compounds with a structure very similar to nitrate/nitrite like phosphate, thiophosphate, dithiophosphate, sulphate, thiosulfate or tetrathionate, among others. Furthermore, the analyses of PacN-LBD and Dd15070 (Gálvez-Roldán et al., 2022) underline the nitrate/nitrite specificity of NIT domains. However, the failure of both ligands to bind to the NIT domain of *P. aeruginosa* chemoreceptor PA4520 indicated that not all family members bind these ligands. We showed here that the mutation of one of the arginine residues predicted to be involved in ligand binding abolished nitrate and nitrite binding (Figure 7). Since this arginine is not conserved in PA4520 (Figure S1), the lacking conservation of this residue may be a way to identify NIT proteins that do not bind nitrate/nitrite. Unfortunately, ligand screening to identify PA4520 ligands were unsuccessful and further research is required to identify the signal that activates this chemoreceptor.

With a maximal response of about 180,000 cells per capillary (Figure 8), the magnitude of nitrate chemotaxis observed was very

strong and well superior to the taxis mediated by the other three characterised *P. atrosepticum* SCRI1043 chemoreceptors PacA, PacB and PacC, that was quantified using the same assay. Whereas PacA-mediated responses to different quaternary amines and proline (Matilla, Velando, Tajuelo, et al., 2022), PacB and PacC responded to different amino acids (Velando et al., 2023). For example, maximal response for nitrate were 15-fold higher than PacA-mediated responses and 7-fold higher compared to a strain in which the PacA concentration was increased by overexpressing its gene *in trans* (Matilla, Velando, Tajuelo, et al., 2022). The magnitude of nitrate chemotaxis was also superior to that mediated by the other characterised NIT-containing chemoreceptor, Dd15070 of *D. dadantii* (Gálvez-Roldán et al., 2022). The magnitude of nitrate response may indicate a particular physiological relevance. Chemotaxis experiments also showed that maximal responses of *P. atrosepticum* to nitrate were about 13-fold higher as compared to those for nitrite (Figure 8). In vitro binding studies showed that the nitrate affinity of the PacN-LBD was only about three-fold greater than that of nitrite (Table 1), suggesting that nitrate binding may generate a molecular stimulus that more efficiently triggers downstream signalling. However, the preferential chemotactic response to nitrate observed for *P. atrosepticum* may not be a general feature since chemotactic responses of *D. dadantii* occurred with a slight preference for nitrite (Gálvez-Roldán et al., 2022).

Taken together, the specificity of the NIT domains for nitrate and nitrite, as well as the wide phylogenetic distribution of this sensor domain, highlights the important role of nitrate- and nitrite-mediated signalling in the regulation of diverse cellular responses in both eukaryotes and prokaryotes.

4 | MATERIALS AND METHODS

4.1 | Strains, plasmids and oligonucleotides

The strains and plasmids used are detailed in Table S3, whereas oligonucleotides used are provided in Table S4.

4.2 | Bioinformatic analyses

15,428 protein entries were retrieved from the UniProtKB database (UniProt Consortium, 2023) with a query for the NIT PFAM family (search term: [xref:pfam-PF08376]). A custom Python3 script was then implemented to extract all PFAM domains and the Taxonomic Identifier (taxid) of the host species annotated in each of the NIT Uniprot entries. The ETE toolkit (Huerta-Cepas et al., 2016) Python framework was then used to query the Taxonomy Browser (NCBI) (Schoch et al., 2020) for the full lineage of each species, and protein entries were then classified by phyla. Phyla with the highest number of annotated NIT entries (Pseudomonadota and Actinomycetota) were further classified into their taxonomic classes and the Actinomycetes class into their orders. To evaluate the abundance of NIT domain-containing proteins in each taxon, the total number

of entries per taxon was determined by queries in UniProtKB using the taxon taxid as query term. A taxonomic tree showing the phyla, Pseudomonadota and Actinomycetota classes, and Actinomycetes orders that contained at least 1 NIT protein was constructed by the CommonTree tool of the NCBI Taxonomy Browser and represented with iTOL v6.

4.3 | Construction of protein expression plasmids

Plasmid pET28_ECA_RS02210-LBD encoding the LBD of chemoreceptor ECA_RS02210 (PacN) of *Pectobacterium atrosepticum* SCRI1043 (residues 28 to 313) was purchased from GenScript. The DNA fragment encoding the LBD of chemoreceptor PSA3335_RS14925 (PscN) of *P. savastanoi* pv. *savastanoi* NCPPB 3335 (residues 32 to 297) was amplified by PCR using genomic DNA and primers specified in Table S4, which contained restriction sites for NdeI and BamHI. The resulting product was digested with these enzymes and cloned into the expression plasmid pET28b(+) to generate pMAMV248. The insert was confirmed by PCR and sequencing.

4.4 | Generation of a mutant in ECA_RS02210 (PacN)

A chromosomal mutant of *P. atrosepticum* SCRI1043 was constructed by homologous recombination using a derivative plasmid of the suicide vector pKNG101. The up- and downstream flanking regions of the *pacN* gene were PCR amplified using the primers detailed in Table S4. The resulting PCR products were digested with EcoRI and PstI and ligated in a three-way ligation into pUC18Not, producing plasmid pUC18Not-ECA_RS02210. Subsequently, a 2.1 kb fragment of this plasmid was subcloned into the marker exchange vector pKNG101 using NotI, resulting in pKNG-ECA_RS02210. This plasmid was transferred into *P. atrosepticum* SRCI1043 by biparental conjugation using *E. coli* β2163. Mutant strains were selected by the failure to grow on 10% (w/v) sucrose-containing agar plates. The integrity of plasmids was verified by DNA sequencing and the deletion of the gene was confirmed by PCR.

4.5 | Quantitative capillary chemotaxis assays

Chemotaxis assays were conducted as reported in Martín-Mora et al., (2019).

4.6 | Overexpression and purification of proteins

4.6.1 | PacN-LBD

Overnight cultures of *Escherichia coli* BL21(DE3) containing pET28_ECA_RS02210-LBD were used to inoculate 500-mL LB medium

supplemented with 50 μg/mL kanamycin in 2-l Erlenmeyer flasks. Cultures were grown at 30°C until an OD_{660} of 0.5, at which point protein production was induced by adding 0.1 mM isopropyl-thiogalactopyranoside (IPTG). The growth temperature was lowered to 18°C and after overnight growth, cells were harvested by centrifugation at 20,000×*g* for 1 h and frozen at −80°C. Cells from a 0.6 L culture were resuspended in 35 mL buffer A (20 mM Tris/HCl, 10 mM imidazole, 5% (v/v) glycerol, 150 mM NaCl, pH 8.0) and broken by French press treatment at 1000 psi (piston diameter of 2.5 cm). After centrifugation at 8500×*g* for 1 h, the supernatant was loaded onto a 5 mL HisTrap column (Amersham Bioscience), washed with five column volumes of buffer A, washed with buffer A containing 40 mM of imidazole and eluted with a 40–500 mM imidazole gradient in buffer A. The protein was dialyzed into analysis buffer (20 mM Tris/HCl, 10% (v/v) glycerol, pH 8.0) for immediate analysis.

4.6.2 | PscN-LBD

E. coli BL21-AI was transformed with pMAMV248 and the resulting strain was grown in 2 L Erlenmeyer flasks containing 400 mL LB medium supplemented with 50 μg/mL kanamycin at 30°C. At an OD_{660} of 0.5, the growth temperature was lowered to 18°C and protein expression was induced by adding 0.2% (w/v) L-arabinose and 0.5 mM IPTG. Growth was continued at 18°C overnight and cells were harvested by centrifugation at 20,000×*g*. Cell pellets derived from 0.6 L culture were resuspended in 35 mL buffer B (30 mM Tris/HCl, 0.3 M NaCl, 10 mM imidazole, 10% (v/v) glycerol, pH 8.0), broken by French press treatment at 1000 psi and centrifuged at 8500×*g* for 1 h. The supernatant was passed through a 0.22 μm cut-off filter (Whatman) and loaded onto a 5-ml HisTrap HP column previously equilibrated in buffer B. Protein was eluted by applying a 45 mM to 500 mM imidazole gradient in buffer B. Pooled fractions were dialyzed into analysis buffer (50 mM K_2HPO_4/KH_2PO_4, 10% (v/v) glycerol, pH 8.0) for immediate analyses.

4.6.3 | PA4520-LBD

The LBD of the PA4520 chemoreceptor from *P. aeruginosa* PAO1 was purified as reported previously (Martín-Mora et al., 2019).

4.7 | Site-directed mutagenesis

An overlapping PCR approach was used to generate the PscN-LBD R182A mutant. Briefly, two amplicons were obtained using the primer pairs RS14925_NIT-NdeI-F /NIT_Arg_R and NIT_Arg-F/RS14925_NIT_BamHI-R (Table S4) and plasmid pMAMV248 as template. These oligonucleotides were designed to replace the codon CGC (R182) with GCC (A182). Using a mixture of the two resulting PCR fragments as template, a 801-bp amplicon was obtained using primers RS14925_NIT-NdeI-F and RS14925_NIT_BamHI-R. This

PCR fragment was subsequently cloned into NdeI/BamHI sites of the expression vector pET28b(+) to generate pMAMV336. The replacement and the absence of further mutations were confirmed by DNA sequencing.

4.8 | Thermal shift assays

Thermal shift assays were performed using a BioRad MyIQ2 Real-Time PCR instrument. Ligands were prepared by dissolving Biolog Phenotype Microarray compounds in 50 μL of Milli-Q water to obtain a final concentration of around 10–20 mM (according to the information of the manufacturer). Screening was performed with compound arrays from Biolog Inc. (Hayward, CA, USA). Each 25 μL assay mixture contained 15 μM protein in their respective analysis buffer and SYPRO™ Orange (Life Technologies) at 5× concentration. Aliquots of 2.5 μL of the resuspended Biolog compounds were added to each well. Samples were heated from 23 to 85°C at a scan rate of 0.5°C/min. The protein unfolding curves were monitored by detecting changes in SYPRO™ Orange fluorescence. Melting temperatures were determined using the first derivative values from the raw fluorescence data.

4.9 | Isothermal titration calorimetry

Measurements were done using a VP-microcalorimeter (MicroCal, Northampton, MA) at 20°C. Proteins at 13–20 μM were placed into the sample cell and titrated with 0.4 to 5 mM of ligand solutions prepared in dialysis buffer immediately before use. The mean enthalpies measured from the injection of ligands into the buffer were subtracted from raw titration data prior to data analysis with the MicroCal version of ORIGIN. Data were fitted with the 'one binding site model'.

4.10 | Differential scanning calorimetry

Studies were performed on a capillary VP-DSC differential scanning calorimeter (Malvern Instruments) with a cell volume of 0.134 mL. Scans were performed at 2–3°C·min⁻¹ over a temperature range of 5–70°C using 20 μM protein. In some experiments, $NaNO_3$ or $NaNO_2$ were added to a final concentration up to 100 μM. Ligand stock solutions were prepared in the analysis buffer. Several buffer-buffer baselines were obtained before each protein run to ascertain proper equilibration of the instrument.

4.11 | Circular dichroism spectroscopy

Experiments were performed on a Jasco J-715 (Tokyo, Japan) spectropolarimeter equipped with a thermostatised cell holder. Measurements of the far-UV CD spectra (260–200 nm) were made

with a 1 mm path-length quartz cuvette. NaNO$_2$ or NaNO$_3$ were added to a final concentration of 100 μM. The resulting spectra were the average of 5 scans at 100 nm/min using 1 nm step resolution, 1 s response and 1 nm bandwidth. The spectra were corrected by the baselines obtained from the corresponding buffer. In order to determine the relative abundance of secondary structure elements, spectra were deconvoluted using the CDNN software package (Bohm et al., 1992).

4.12 | Analytical ultracentrifugation

Experiments were performed in a Beckman Coulter Optima XL-I analytical ultracentrifuge (Beckman Coulter, Palo Alto, CA, USA) equipped with UV–visible absorbance and interference optics detection systems. An An50Ti 8-hole rotor and 12 mm path-length charcoal-filled epon double-sector centrepieces were used. The experiments were carried out at 10°C, using samples in 50 mM K$_2$HPO$_4$/KH$_2$PO$_4$ at pH 7.5. Protein at 5 μM to 20 μM was analysed in the absence and presence of 1 mM NaNO$_3$ or NaNO$_2$. Sedimentation-velocity (SV) runs were carried out at a rotor speed of 48,000 rpm using 400 μL samples and dialysis buffer as reference. A laser at 235 nm was used in the absorbance optics mode. A least squares boundary modelling of the SV data was used to calculate sedimentation-coefficient distributions with the size-distribution *c(s)* method (Schuck, 2000) implemented in the SEDFIT v14.1 software. The molecular weight was extracted from the sedimentation profiles, via the Lamm equation solution included in the *c(s)* model of SEDFIT. The best-fit values obtained for the sedimentation coefficient (*s*, in S or Svedbergs) and diffusion were used to estimate the molar mass of the molecule using the Svedberg equation. Buffer density ($\rho = 1.0071$ g/mL) and viscosity ($\eta = 0.01331$ Poise) at 10°C were estimated by SEDNTERP software (Laue et al., 1992) from the buffer components. The partial specific volume used was 0.7242 mL/g as calculated from the amino acid sequence also using SEDNTERP software. The sequence-derived molecular mass of the monomer PscN-LBD was 31.8 kDa.

AUTHOR CONTRIBUTIONS

Elizabet Monteagudo-Cascales: Investigation; Validation; Visualization; Writing - review & editing. álvaro Ortega: Investigation; Validation; Visualization; Writing - review & editing. Félix Velando: Investigation; Validation; Visualization; Writing - review & editing. Bertrand Morel: Investigation; Validation; Visualization; Writing - review & editing. Miguel A. Matilla: Conceptualization; Investigation; Validation; Visualization; Writing - review & editing; Funding acquisition; Supervision; Project administration. Tino Krell: Writing - original draft; Funding acquisition; Supervision; Validation; Visualization; Writing - review & editing; Project administration.

CONFLICT OF INTEREST STATEMENT

None.

ETHICS STATEMENT

This article does not contain any studies with human participants or animals.

DATA AVAILABILITY STATEMENT

The data that supports the findings of this study are available in the supplementary material of this article.

ORCID

Tino Krell https://orcid.org/0000-0002-9040-3166

REFERENCES

Biemann, H.P. & Koshland, D.E., Jr. (1994) Aspartate receptors of Escherichia coli and salmonella typhimurium bind ligand with negative and half-of-the-sites cooperativity. *Biochemistry*, 33, 629–634.

Bohm, G., Muhr, R. & Jaenicke, R. (1992) Quantitative analysis of protein far UV circular dichroism spectra by neural networks. *Protein Engineering*, 5, 191–195.

Boudes, M., Lazar, N., Graille, M., Durand, D., Gaidenko, T.A., Stewart, V. et al. (2012) The structure of the NasR transcription antiterminator reveals a one-component system with a NIT nitrate receptor coupled to an ANTAR RNA-binding effector. *Molecular Microbiology*, 85, 431–444.

Caldas, T., Demont-Caulet, N., Ghazi, A. & Richarme, G. (1999) Thermoprotection by glycine betaine and choline. *Microbiology (Reading)*, 145(Pt 9), 2543–2548.

Cerna-Vargas, J.P., Santamaría-Hernando, S., Matilla, M.A., Rodríguez-Herva, J.J., Daddaoua, A., Rodríguez-Palenzuela, P. et al. (2019) Chemoperception of specific amino acids controls phytopathogenicity in Pseudomonas syringae pv. tomato. *mBio*, 10, e01868-19.

Chen, C. & Beattie, G.A. (2008) Pseudomonas syringae BetT is a low-affinity choline transporter that is responsible for superior osmoprotection by choline over glycine betaine. *Journal of Bacteriology*, 190, 2717–2725.

Clarke, S. & Koshland, D.E., Jr. (1979) Membrane receptors for aspartate and serine in bacterial chemotaxis. *The Journal of Biological Chemistry*, 254, 9695–9702.

Colin, R., Ni, B., Laganenka, L. & Sourjik, V. (2021) Multiple functions of flagellar motility and chemotaxis in bacterial physiology. *FEMS Microbiology Reviews*, 45, fuab038.

Derbyshire, E.R. & Marletta, M.A. (2012) Structure and regulation of soluble guanylate cyclase. *Annual Review of Biochemistry*, 81, 533–559.

Elgamoudi, B.A., Andrianova, E.P., Shewell, L.K., Day, C.J., King, R.M., Taha, R.H. et al. (2021) The *Campylobacter jejuni* chemoreceptor Tlp10 has a bimodal ligand-binding domain and specificity for multiple classes of chemoeffectors. *Science Signaling*, 14, eabc8521.

Fernández, M., Matilla, M.A., Ortega, Á. & Krell, T. (2017) Metabolic value Chemoattractants are preferentially recognized at broad ligand range chemoreceptor of Pseudomonas putida KT2440. *Frontiers in Microbiology*, 8, 990.

Foster, D.L., Mowbray, S.L., Jap, B.K. & Koshland, D.E., Jr. (1985) Purification and characterization of the aspartate chemoreceptor. *The Journal of Biological Chemistry*, 260, 11706–11710.

Galperin, M.Y. (2018) What bacteria want. *Environmental Microbiology*, 20, 4221–4229.

Gálvez-Roldán, C., Cerna-Vargas, J.P., Rodriguez Herva, J.J., Krell, T., Santamaria-Hernando, S. & López-Solanilla, E. (2022) A NIT sensor domain containing chemoreceptor is required for a successful entry and virulence of Dickeya dadantii 3937 in potato plants. *Phytopathology*, 113, 390–399. Available from: https://doi.org/10.1094/PHYTO-10-22-0367-R

Gavira, J.A., Ortega, Á., Martín-Mora, D., Conejero-Muriel, M.T., Corral-Lugo, A., Morel, B. et al. (2018) Structural basis for polyamine binding at the dCACHE domain of the McpU chemoreceptor from pseudomonas putida. *Journal of Molecular Biology*, 430, 1950–1963.

Gumerov, V.M., Ortega, D.R., Adebali, O., Ulrich, L.E. & Zhulin, I.B. (2020) MiST 3.0: an updated microbial signal transduction database with an emphasis on chemosensory systems. *Nucleic Acids Research*, 48, D459–D464.

Gushchin, I., Melnikov, I., Polovinkin, V., Ishchenko, A., Yuzhakova, A., Buslaev, P. et al. (2017) Mechanism of transmembrane signaling by sensor histidine kinases. *Science*, 356, 356:eaah6345.

Ha, S.H. & Ferrell, J.E. (2016) Thresholds and ultrasensitivity from negative cooperativity. *Science*, 352, 990–993.

Hida, A., Oku, S., Nakashimada, Y., Tajima, T. & Kato, J. (2017) Identification of boric acid as a novel chemoattractant and elucidation of its chemoreceptor in Ralstonia pseudosolanacearum Ps29. *Scientific Reports*, 7, 8609.

Huerta-Cepas, J., Serra, F. & Bork, P. (2016) ETE 3: reconstruction, analysis, and visualization of phylogenomic data. *Molecular Biology and Evolution*, 33, 1635–1638.

Jumper, J., Evans, R., Pritzel, A., Green, T., Figurnov, M., Ronneberger, O. et al. (2021) Highly accurate protein structure prediction with AlphaFold. *Nature*, 596, 583–589.

Kraft, B., Strous, M. & Tegetmeyer, H.E. (2011) Microbial nitrate respiration—genes, enzymes and environmental distribution. *Journal of Biotechnology*, 155, 104–117.

Kutvonen, H., Rajala, P., Carpén, L. & Bomberg, M. (2015) Nitrate and ammonia as nitrogen sources for deep subsurface microorganisms. *Frontiers in Microbiology*, 6, 1079.

Lacal, J., Alfonso, C., Liu, X., Parales, R.E., Morel, B., Conejero-Lara, F. et al. (2010) Identification of a chemoreceptor for tricarboxylic acid cycle intermediates: differential chemotactic response towards receptor ligands. *The Journal of Biological Chemistry*, 285, 23126–23136.

Laue, T.M., Shah, B.D., Ridgeway, T.M. & Pelletier, S.L. (1992) Computer-aided interpretation of analytical sedimentation data for proteins. In: Harding, S.E., Horton, J.C. & Rowe, A.J. (Eds.) *Analytical ultracentrifugation in biochemistry and polymer science*. Cambridge, UK: Royal Society of Chemistry, pp. 90–125.

Mansfield, J., Genin, S., Magori, S., Citovsky, V., Sriariyanum, M., Ronald, P. et al. (2012) Top 10 plant pathogenic bacteria in molecular plant pathology. *Molecular Plant Pathology*, 13, 614–629.

Martín-Mora, D., Ortega, Á., Matilla, M.A., Martínez-Rodríguez, S., Gavira, J.A. & Krell, T. (2019) The molecular mechanism of nitrate chemotaxis via direct ligand binding to the PilJ domain of McpN. *mBio*, 10, e02334–e02318.

Martin-Mora, D., Ortega, A., Reyes-Darias, J.A., Garcia, V., Lopez-Farfan, D., Matilla, M.A. et al. (2016) Identification of a chemoreceptor in *Pseudomonas aeruginosa* that specifically mediates chemotaxis toward alpha-ketoglutarate. *Frontiers in Microbiology*, 7, 1937.

Martin-Rodriguez, A.J., Higdon, S.M., Thorell, K., Tellgren-Roth, C., Sjoling, A., Galperin, M.Y. et al. (2022) Comparative genomics of cyclic di-GMP metabolism and chemosensory pathways in Shewanella algae strains: novel bacterial sensory domains and functional insights into lifestyle regulation. *mSystems*, 7, e0151821.

Matas, I.M., Lambertsen, L., Rodríguez-Moreno, L. & Ramos, C. (2012) Identification of novel virulence genes and metabolic pathways required for full fitness of *Pseudomonas savastanoi* pv. *savastanoi* in olive (Olea europaea) knots. *The New Phytologist*, 196, 1182–1196.

Matilla, M.A. & Krell, T. (2018) The effect of bacterial chemotaxis on host infection and pathogenicity. *FEMS Microbiology Reviews*, 42, 40–67.

Matilla, M.A., Velando, F., Martín-Mora, D., Monteagudo-Cascales, E. & Krell, T. (2022) A catalogue of signal molecules that interact with sensor kinases, chemoreceptors and transcriptional regulators. *FEMS Microbiology Reviews*, 46, fuab043.

Matilla, M.A., Velando, F., Tajuelo, A., Martín-Mora, D., Xu, W., Sourjik, V. et al. (2022) Chemotaxis of the human pathogen *Pseudomonas aeruginosa* to the neurotransmitter acetylcholine. *mBio*, 13, e0345821.

Meadows, J.A. & Wargo, M.J. (2015) Carnitine in bacterial physiology and metabolism. *Microbiology (Reading)*, 161, 1161–1174.

Milligan, D.L. & Koshland, D.E., Jr. (1993) Purification and characterization of the periplasmic domain of the aspartate chemoreceptor. *The Journal of Biological Chemistry*, 268, 19991–19997.

Mistry, J., Chuguransky, S., Williams, L., Qureshi, M., Salazar, G.A., Sonnhammer, E.L.L. et al. (2021) Pfam: the protein families database in 2021. *Nucleic Acids Research*, 49, D412–D419.

Monteagudo-Cascales, E., Martín-Mora, D., Xu, W., Sourjik, V., Matilla, M.A., Ortega, Á. et al. (2022) The pH robustness of bacterial sensing. *mBio*, 13, e0165022.

Moroz, L.L., Romanova, D.Y. & Kohn, A.B. (2021) Neural versus alternative integrative systems: molecular insights into origins of neurotransmitters. *Philosophical Transactions of the Royal Society of London. Series B, Biological Sciences*, 376, 20190762.

Moroz, L.L., Romanova, D.Y., Nikitin, M.A., Sohn, D., Kohn, A.B., Neveu, E. et al. (2020) The diversification and lineage-specific expansion of nitric oxide signaling in placozoa: insights in the evolution of gaseous transmission. *Scientific Reports*, 10, 13020.

Ottemann, K.M. & Koshland, D.E. (1997) Converting a transmembrane receptor to a soluble receptor: recognition domain to effector domain signaling after excision of the transmembrane domain. *Proceedings of the National Academy of Sciences of the United States of America*, 94, 11201–11204.

Pineda-Molina, E., Reyes-Darias, J.-A., Lacal, J., Ramos, J.L., García-Ruiz, J.M., Gavira, J.A. et al. (2012) Evidence for chemoreceptors with bimodular ligand-binding regions harboring two signal-binding sites. *Proceedings of the National Academy of Sciences of the United States of America*, 109, 18926–18931.

Ramos, C., Matas, I.M., Bardaji, L., Aragon, I.M. & Murillo, J. (2012) *Pseudomonas savastanoi* pv. *savastanoi*: some like it knot. *Molecular Plant Pathology*, 13, 998–1009.

Rico-Jiménez, M., Muñoz-Martínez, F., García-Fontana, C., Fernandez, M., Morel, B., Ortega, A. et al. (2013) Paralogous chemoreceptors mediate chemotaxis towards protein amino acids and the non-protein amino acid gamma-aminobutyrate (GABA). *Molecular Microbiology*, 88, 1230–1243.

Ringrose, J.H., van den Toorn, H.W.P., Eitel, M., Post, H., Neerincx, P., Schierwater, B. et al. (2013) Deep proteome profiling of Trichoplax adhaerens reveals remarkable features at the origin of metazoan multicellularity. *Nature Communications*, 4, 1408.

Sakata, N. & Ishiga, Y. (2023) Prevention of stomatal entry as a strategy for plant disease control against foliar pathogenic pseudomonas species. *Plants (Basel)*, 12, 590.

Sanchis-López, C., Cerna-Vargas, J.P., Santamaría-Hernando, S., Ramos, C., Krell, T., Rodríguez-Palenzuela, P. et al. (2021) Prevalence and specificity of chemoreceptor profiles in plant-associated bacteria. *mSystems*, 6, e0095121.

Schierwater, B., Osigus, H.-J., Bergmann, T., Blackstone, N.W., Hadrys, H., Hauslage, J. et al. (2021) The enigmatic Placozoa part 1: exploring evolutionary controversies and poor ecological knowledge. *BioEssays*, 43, e2100080.

Schoch CL, Ciufo S, Domrachev M, Hotton CL, Kannan S, Khovanskaya R, Leipe D, McVeigh R, O'Neill K, Robbertse B, Sharma S, Soussov V, Sullivan JP, Sun L, Turner S, Karsch-Mizrachi I. 2020. NCBI

taxonomy: a comprehensive update on curation, resources and tools. *Database: The Journal of Biological Databases and Curation*, *2020*, 1–21.

Schuck, P. (2000) Size-distribution analysis of macromolecules by sedimentation velocity ultracentrifugation and Lamm equation modeling. *Biophysical Journal*, *78*, 1606–1619.

Shoun, H., Kano, M., Baba, I., Takaya, N. & Matsuo, M. (1998) Denitrification by actinomycetes and purification of dissimilatory nitrite reductase and azurin from Streptomyces thioluteus. *Journal of Bacteriology*, *180*, 4413–4415.

Shu, C.J., Ulrich, L.E. & Zhulin, I.B. (2003) The NIT domain: a predicted nitrate-responsive module in bacterial sensory receptors. *Trends in Biochemical Sciences*, *28*, 121–124.

Smith, C.L., Varoqueaux, F., Kittelmann, M., Azzam, R.N., Cooper, B., Winters, C.A. et al. (2014) Novel cell types, neurosecretory cells, and body plan of the early-diverging metazoan *Trichoplax adhaerens*. *Current Biology*, *24*, 1565–1572.

Toth, I.K. (2022) Microbe profile: *Pectobacterium atrosepticum*: an enemy at the door. *Microbiology (Reading)*, *168*, 1–3.

Tunchai, M., Hida, A., Oku, S., Tajima, T. & Kato, J. (2021) Chemotactic disruption as a method to control bacterial wilt caused by Ralstonia pseudosolanacearum. *Bioscience, Biotechnology, and Biochemistry*, *85*, 697–702.

Ulrich, L.E. & Zhulin, I.B. (2005) Four-helix bundle: a ubiquitous sensory module in prokaryotic signal transduction. *Bioinformatics*, *21*, Supplement 3, iii45–iii48.

UniProt Consortium. (2023) UniProt: the universal protein knowledgebase in 2023. *Nucleic Acids Research*, *51*, D523–D531.

Upadhyay, A.A., Fleetwood, A.D., Adebali, O., Finn, R.D. & Zhulin, I.B. (2016) Cache domains that are homologous to, but different from PAS domains comprise the largest superfamily of extracellular sensors in prokaryotes. *PLoS Computational Biology*, *12*, e1004862.

van Bergeijk, D.A., Terlouw, B.R., Medema, M.H. & van Wezel, G.P. (2020) Ecology and genomics of actinobacteria: new concepts for natural product discovery. *Nature Reviews. Microbiology*, *18*, 546–558.

Varoqueaux, F. & Fasshauer, D. (2017) Getting nervous: an evolutionary overhaul for communication. *Annual Review of Genetics*, *51*, 455–476.

Varoqueaux, F., Williams, E.A., Grandemange, S., Truscello, L., Kamm, K., Schierwater, B. et al. (2018) High cell diversity and complex Peptidergic signaling underlie placozoan behavior. *Current Biology*, *28*, 3495–3501.e2.

Velando, F., Matilla, M.A., Zhulin, I.B. & Krell, T. (2023) Three unrelated chemoreceptors provide *Pectobacterium atrosepticum* with a broad-spectrum amino acid sensing capability. *Microbial Biotechnology*. Online ahead of print. Available from: https://doi.org/10.1111/1751-7915.14255

Yañez-Guerra, L.A., Thiel, D. & Jékely, G. (2022) Premetazoan origin of neuropeptide signaling. *Molecular Biology and Evolution*, *39*, msac051.

Yu, D., Ma, X., Tu, Y. & Lai, L. (2015) Both piston-like and rotational motions are present in bacterial chemoreceptor signaling. *Scientific Reports*, *5*, 8640.

Zhang, H., Ma, B., Huang, T. & Shi, Y. (2021) Nitrate reduction by the aerobic denitrifying actinomycete Streptomyces sp. XD-11-6-2: performance, metabolic activity, and micro-polluted water treatment. *Bioresource Technology*, *326*, 124779.

Zhang, W., Olson, J.S. & Phillips, G.N., Jr. (2005) Biophysical and kinetic characterization of HemAT, an aerotaxis receptor from Bacillus subtilis. *Biophysical Journal*, *88*, 2801–2814.

SUPPORTING INFORMATION

Additional supporting information can be found online in the Supporting Information section at the end of this article.